Spectral implementation of some quantum algorithms by one- and two-dimensional nuclear magnetic resonance

Ranabir Das
Department of Physics, Indian Institute of Science, Bangalore-560012, India

Anil Kumar[a)]
Department of Physics and Sophisticated Instruments Facility, Indian Institute of Science, Bangalore-560012, India

Quantum information processing has been effectively demonstrated on a small number of qubits by nuclear magnetic resonance. An important subroutine in any computing is the readout of the output. ''Spectral implementation'' originally suggested by Z. L. Madi, R. Bruschweiler, and R. R. Ernst [J. Chem. Phys. **109**, 10603 (1999)], provides an elegant method of readout with the use of an extra ''observer'' qubit. At the end of computation, detection of the observer qubit provides the output via the multiplet structure of its spectrum. In spectral implementation by two-dimensional experiment the observer qubit retains the memory of input state during computation, thereby providing correlated information on input and output, in the same spectrum. Spectral implementation of Grover's search algorithm, approximate quantum counting, a modified version of Berstein-Vazirani problem, and Hogg's algorithm are demonstrated here in three- and four-qubit systems.

I. INTRODUCTION

In 1982 Feynmann pointed out that it would be more efficient to simulate the behavior of a quantum system using a quantum, rather than a classical device.[1] The idea of a purpose-built quantum computer, which could simulate the physical behavior of a quantum system as well as perform certain tasks much faster than classical computer, attracted immediate attention.[2,3] The theory of such quantum computers is now well understood and several quantum algorithms like Deutsch-Jozsa (DJ) algorithm, Grover's search algorithm, Shor's factorization algorithm, Berstein-Vazirani problem, Hogg's algorithm and quantum counting have been developed.[4–10]

However, building a realistic large-scale quantum computer has been extremely challenging.[11,12] Various devices are being examined for building a quantum information processing (QIP) device which is coherent and unitary.[11] Among these, nuclear magnetic resonance (NMR) has shown great promise by demonstrating several quantum algorithms and other QIP tasks on small-scale devices.[13–28] The last step in any quantum information processing task is the ''readout'' of the output. Typically in NMR, the readout is obtained by selectively detecting spins,[29] or by mapping out the full density matrix.[30–32] It was first pointed out by Ernst and co-workers[33] that it is advantageous from the spectroscopic viewpoint that quantum states can be assigned to individual spectral lines, corresponding to transitions between energy levels rather than to the energy levels themselves.[33] However, for such an advantage one has to use an extra qubit called ''observer'' qubit. After computation the readout is obtained by detecting only the observer qubit, whose multiplet spectrum provides the result of the computation carried out on the work qubits. Such a ''spectral implementation'' of a quantum computer was demonstrated by implementation of some logic gates by one- and two-dimensional NMR.[33] Later, spectral implementation of a complete set of logic gates and DJ-algorithm,[34] Berstein-Vazirani problem,[35] and quantum Fourier transform[36] have also been implemented by NMR. In this work we extend this range by spectrally implementing Grover's search algorithm, approximate quantum counting, a modified version of Berstein-Vazirani problem, and Hogg's algorithm. All the algorithms are implemented by both one- and two-dimensional NMR.

II. THEORY

A convenient representation of the density matrices of pure states in Liouville space can be obtained by the polarization operators for each qubit (k),[33,37]

$$
\begin{aligned}
&I_0^k=|0\rangle\langle 0|=\begin{pmatrix}1&0\\0&0\end{pmatrix}, \quad I_1^k=|1\rangle\langle 1|=\begin{pmatrix}0&0\\0&1\end{pmatrix},\\
&I_+^k=|0\rangle\langle 1|=\begin{pmatrix}0&1\\0&0\end{pmatrix}, \quad I_-^k=|1\rangle\langle 0|=\begin{pmatrix}0&0\\1&0\end{pmatrix},\\
&I_x^k=\frac{1}{2}(I_+^k+I_-^k)=\frac{1}{2}\begin{pmatrix}0&1\\1&0\end{pmatrix},\\
&I_y^k=\frac{1}{2i}(I_+^k-I_-^k)=\frac{1}{2i}\begin{pmatrix}0&1\\-1&0\end{pmatrix},\\
&I_z^k=\frac{1}{2}(I_0^k-I_1^k)=\frac{1}{2}\begin{pmatrix}1&0\\0&-1\end{pmatrix}.
\end{aligned}
\tag{1}
$$

For example, the density matrix of a pure state $|00\rangle+|11\rangle$ can be expressed as

[a)]DAE-BRNS Senior Scientist.

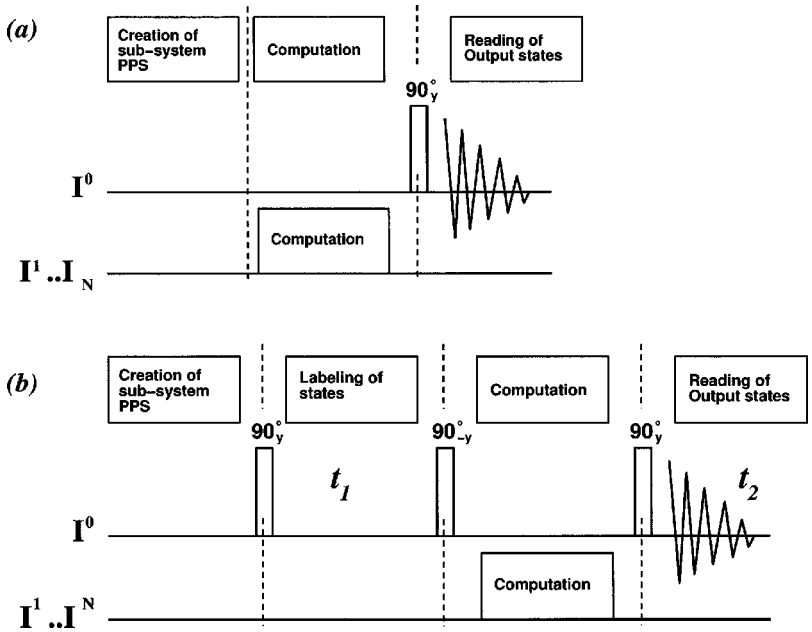

FIG. 1. Experimental protocol for spectral implementation of quantum algorothms (Ref. 33). (a) One-dimensional experiment. The first stage is to create an subsystem pseudopure state of the type $I_z^0 I_0^1 I_0^2 \cdots I_0^N$, followed by computation on $I^1 \cdots I^N$ qubits. Finally the transitions of the observer qubit I^0 are detected by a 90_y° pulse. (b) Two-dimensional experiment. After the creation of initial $I_z^0 I_0^1 I_0^2 \cdots I_0^N$ subsystem PPS, the observer qubit is flipped by 90_y° pulse to transverse magnetization and allowed to evolve for a time t_1. During t_1, the transitions of the observer qubit modulate with the frequencies characterized by the input state of the other N qubits. A subsequent 90_{-y}° brings the magnetization back to longitudinal direction. The computation is performed on the $I^1 \cdots I^N$ qubits. The transitions of the observer qubit are finally detected by a 90_y° pulse. A series of experiments are performed with systematic increment of the t_1 period and the collected 2D data set $s(t_1, t_2)$ is Fourier transformed with respectd to t_1 and t_2 to get the 2D spectrum $S(\omega_1, \omega_2)$.

$$\begin{pmatrix} 1 & 0 & 0 & 1 \\ 0 & 0 & 0 & 0 \\ 0 & 0 & 0 & 0 \\ 1 & 0 & 0 & 1 \end{pmatrix} = |00\rangle\langle 00| + |11\rangle\langle 11| + |00\rangle\langle 11| + |11\rangle\langle 00|, \tag{2}$$

$$= I_0^1 I_0^2 + I_1^1 I_1^2 + I_+^1 I_+^2 + I_-^1 I_-^2 . \tag{3}$$

The scheme of spectral implementation of one-dimensional (1D) and two-dimensional (2D) NMR is, respectively, given in Figs. 1(a) and 1(b). We start with the thermal equilibrium density matrix $I_z^0 + I_z^1 + I_z^2 + \cdots + I_z^N$ and in the preparation period we create density matrix of the form $I_z^0 I_0^1 I_0^2 \cdots I_0^N$, where $I_z^0 I_0^1 I_0^2 \cdots I_0^N = (I_0^0 I_0^1 I_0^2 \cdots I_0^N - I_1^0 I_1^1 I_1^2 \cdots I_1^N)/2$. In this state the last $N-1$ qubits are simultaneously in pseudopure state (PPS) (Ref. 13) in two distinct domains of energy levels, in which the observer qubit is in state $|0\rangle$ and $|1\rangle$, respectively. Such a state is known as subsystem pseudopure state.[14] This is further elaborated in Fig. 2.

The schematic diagram of the energy levels and the spectrum of the observer qubit in a three-qubit system, where the first qubit is the observer qubit, is given in Fig. 2. Figure 2(a) shows the equilibrium deviation populations (populations in excess of uniform background population) of various energy levels and Fig. 2(b) the equilibrium spectrum of the observer qubit obtained after a $(\pi/2)$ detection pulse. Each of the spectral lines in the multiplet correspond to the state of the other qubits. The energy level diagram along with the deviation populations after creating the desired initial state of $I_z^0 I_0^1 I_0^2$ is given in Fig. 2(c). The corresponding observer qubit spectrum of Fig. 2(d) has a single line, that of $|00\rangle$, indicating that the other qubits are in $|00\rangle$ state.

Typically after computation, the density matrix is of the form $I_z^0 I_{0/1}^1 I_{0/1}^2 \cdots I_{0/1}^N$, where the subscript 0/1 means that the particular qubit is either in 0 or 1 state. A subsequent $(\pi/2)_y^0$ pulse on the observer (I^0) qubit creates single quantum co-

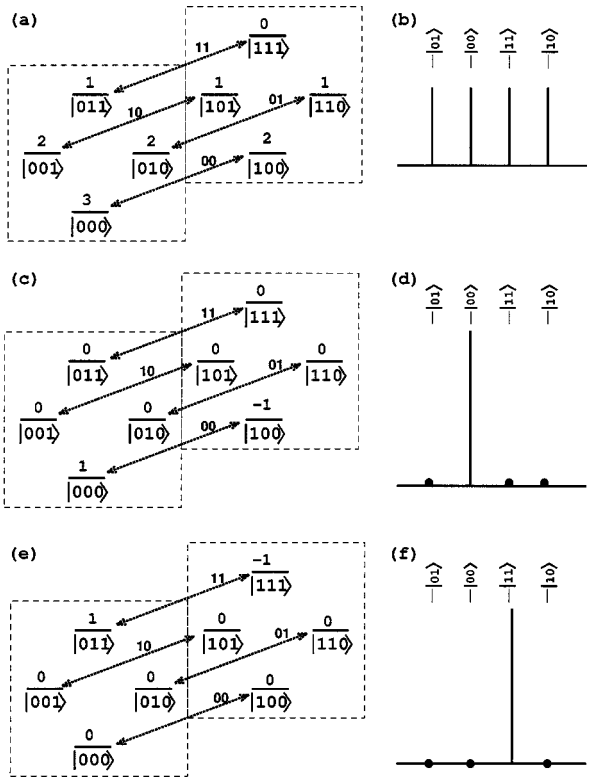

FIG. 2. Schematic diagram of the energy levels and the spectrum of the observer qubit at different stages of spectral implementation. (a) Deviation equlibrium populations. The dotted arrows denote the transitions of observer qubit. (b) Equilibrium spectrum of observer qubit shown by stick diagram. Each transition of the spectrum correspond to the state of other qubits, which are given above each line. (c) Deviation populations after creation of $|00\rangle$ subsystem pseudopure state by POPS. Populations of only $|00\rangle$ eigenstate is nonzero in the two distinct domains of energy levels, where observer qubit is, respectively, in state $|0\rangle$ and $|1\rangle$. (d) Spectrum of observer qubit after creation of POPS. The dots denote null intensity. (e) Deviation populations after a typical computation whose output is $|11\rangle$. (f) Spectrum of observer qubit after such a computation.

herences of the form $I_x^0 I_{0/1}^1 I_{0/1}^2 \cdots I_{0/1}^N$, which gives a single line in the spectrum corresponding to the output state of other qubits. In the example of three-qubit system given in Fig. 2, let us assume that we start with the initial $|00\rangle$ pseudopure state of the qubits (other than observer qubit) and after some computation let the output state be $|11\rangle$. After such a computation, the deviation populations and spectrum of observer qubit are given, respectively, in Figs. 2(e) and 2(f).

In some algorithms however, the output is a superposition of multiple states. Then, the output density matrix will have nonzero populations in all the output states and the coherences between them. The spectrum of the observer qubits will thus have multiple lines, corresponding to all the output states. For example, in the three-qubit system, if the output state of the work qubits is $|00\rangle+|11\rangle$, the density matrix is of the form $I_z^0 I_0^1 I_0^2 + I_z^0 I_1^1 I_1^2 + I_z^0 I_+^1 I_+^2 + I_z^0 I_-^1 I_-^2$. After the $(\pi/2)_y^0$ detection pulse on the observer qubit the single quantum coherences of the terms $I_x^0 I_0^1 I_0^2$ and $I_x^0 I_1^1 I_1^2$ will be detected. The spectrum of the observer qubit will show two lines corresponding to the states of $|00\rangle$ and $|11\rangle$ of the other qubits. The coherences will be converted into multiple quantum coherences which are not detected directly in NMR. Hence, the spectral implementation gives a measure of the deviation populations or probabilities of each state but does not measure the coherences, which if required can be measured by state tomography.[30–32]

A two-dimensional experiment for spectral implementation provides the input and output in the same spectrum. The pulse sequence for the two-dimensional experiment of spectral implementation is given in Fig. 1(b). Suppose a computation starts with the input of $|00\cdots0\rangle$ and end with an output of $|11\cdots1\rangle$ state. After preparation of the initial $I_z^0 I_0^1 I_0^2 \cdots I_0^N$ state the application of the pulse sequence of Fig. 1(b) can be analyzed in the following steps:

$$
\begin{aligned}
I_z^0 I_0^1 I_0^2 \cdots I_0^N &\xrightarrow{(\pi/2)_y^0} I_x^0 I_0^1 I_0^2 \cdots I_0^N \xrightarrow{t_1} I_x^0 I_0^1 I_0^2 \cdots I_0^N \cos(\omega_{00\cdots0}^0 t_1) \\
&\xrightarrow{(\pi/2)_{-y}^0, G_z} I_z^0 I_0^1 I_0^2 \cdots I_0^N \cos(\omega_{00\cdots0}^0 t_1) \\
&\xrightarrow{\text{Comp}} I_z^0 I_1^1 I_1^2 \cdots I_1^N \cos(\omega_{00\cdots0}^0 t_1) \\
&\xrightarrow{(\pi/2)_y^0 - t_2} I_x^0 I_1^1 I_1^2 \cdots I_1^N \cos(\omega_{00\cdots0}^0 t_1) \cos(\omega_{11\cdots1}^0 t_2),
\end{aligned}
\tag{4}
$$

where $\omega_{00\ldots0}^0$ and $\omega_{11\ldots1}^0$ are, respectively, the frequencies of the $|00\ldots0\rangle$ and $|11\ldots1\rangle$ transitions of the observer qubit I^0, $(\pi/2)_y^0$ is a $(\pi/2)$ rotation of the observer qubit (I^0) about y axis, G_z is the gradient pulse and Comp is the computation performed on the work qubits. It may be noted that the signal from the observer qubit is modulated by the frequencies corresponding to both the input and the output states of the work qubits. A series of experiments are performed with systematic increment of the t_1 period followed by detection of the observer qubit's signal. The collected two-dimensional time domain data set $s(t_1,t_2)$ is double Fourier transformed with respect to t_1 and t_2 yielding a two-dimensional frequency domain spectrum $S(\omega_1,\omega_2)$, which contains along ω_1 the input states of work qubits before computation and along ω_2 the output state of work qubits after computation.

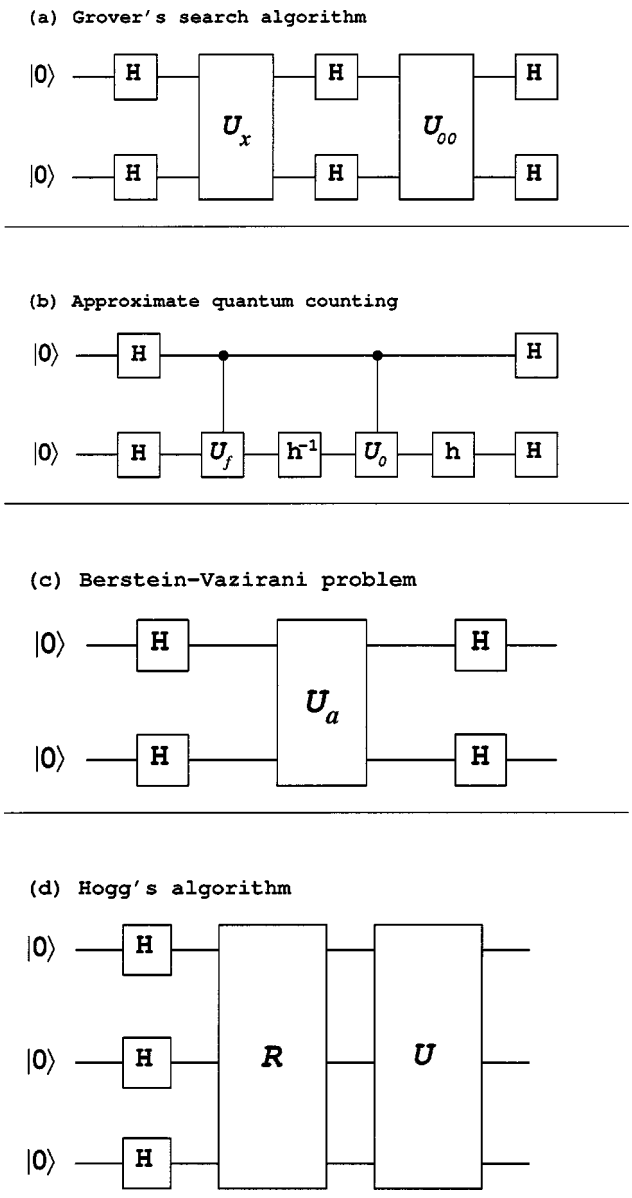

FIG. 3. The quantum circuits of various algorithms. (a) Quantum circuit for implementation of Grover's search algorithm in a two-qubit system. (b) Quantum circuit for implementation of approximate quantum counting in a two-qubit system. (c) Quantum circuit for implementation of Berstein-Vazirani problem. (d) Quantum circuit for implementation of Hogg's algorithm in a three-qubit system.

III. GROVER'S SEARCH ALGORITHM

Grover's search algorithm can search an unsorted database of size N in $O(\sqrt{N})$ steps while a classical search would require $O(N)$ steps.[5] Grover's search algorithm has been earlier demonstrated by NMR.[18,19] The quantum circuit for implementing Grover's search algorithm on two-qubit system is given in Fig. 3(a). The algorithm starts from a $|00\rangle$ pseudopure state. A uniform superposition of all states are

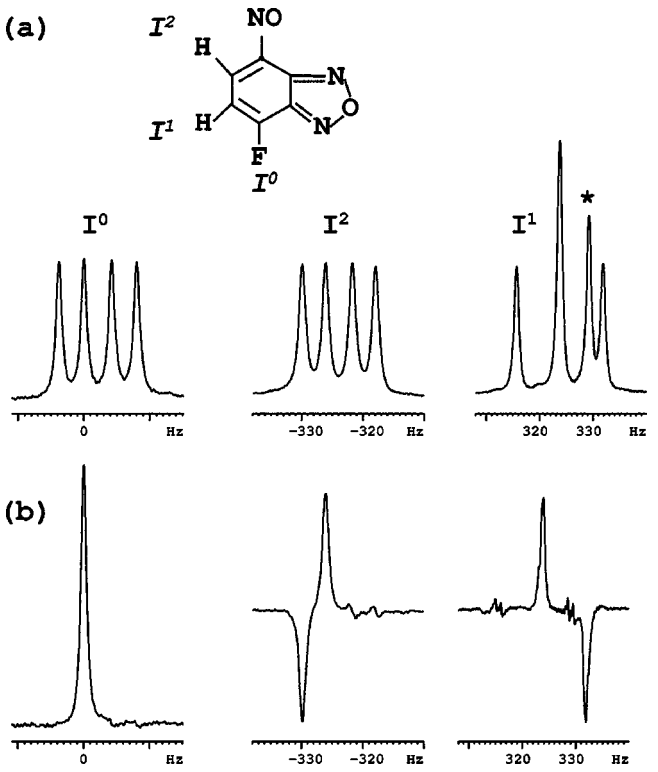

FIG. 4. (a) Chemical structure and equilibrium spectrum of 4-fluro 7-nitro benzofuran. The *J*-coupling values are $J_{01}=-3.84$ Hz, $J_{02}=8.01$ Hz, and $J_{12}=8.07$ Hz. The peak denoted by asterisk (*) belongs to solvent. (b) Spectra after creation of POPS. A Gaussian shaped selective pulse of 500 ms duration was applied on the $|000\rangle\leftrightarrow|100\rangle$ transition and the resultant spectra is subtracted from the equlibrium spectra of figure (a) to yield (b). [See Fig. 2(c)].

created by the initial Hadamard gates (H). Then the sign of the searched state "x" is inverted by the oracle through the operator

$$U_x = I - 2|x\rangle\langle x|. \tag{5}$$

An inversion about mean is performed on all the states by a diffusion operator $HU_{00}H$, where

$$U_{00} = I - 2|00\rangle\langle 00|. \tag{6}$$

For an N-sized database the algorithm requires $O(\sqrt{N})$ iterations of $U_x H U_{00} H$. For a two-qubit system with four states, only one iteration is required. We have implemented this algorithm on the two qubits of a three-qubit system with the third qubit acting as the observer qubit. The three-qubit system chosen for this purpose is 4-fluro 7-nitro benzofuran (dissolved in $CDCl_3$), which comprises of a two protons (^{1}H) and a flourine (^{19}F). The chemical structure of the molecule along with the equilibrium proton and fluorine spectrum is given in Fig. 4(a). We have chosen the fluorine spin as the observer qubit. The Hamiltonian of the system is

$$\mathcal{H} = \sum_{i=0}^{2} 2\pi\nu_i I_z^i + \sum_{i>j} 2\pi J_{ij} I_z^i I_z^j, \tag{7}$$

where ν_i are the resonance frequencies of various spins and J_{ij} are the indirect couplings. The experiments were performed at a field of 11.4 Tesla in a Bruker DRX500 spectrometer. At the magnetic field of 11.4 Tesla, the resonant frequency of proton is 500.13 MHz and that of fluorine is 470.59 MHz. The frequency difference between the two protons is 646 Hz. The J couplings are $J_{01}=-3.84$ Hz, $J_{02}=8.01$ Hz, and $J_{12}=8.07$ Hz. The ^{1}H transmitter frequency is set at the center of the proton spectrum.

The required initial state of $I_z^0|00\rangle\langle 00|$ was prepared by the method of pair of pseudopure states (POPS), originally suggested by Fung.[38,39] The method requires two population distributions, (i) equilibrium populations and (ii) population distribution after a selective (π) pulse on $|000\rangle\leftrightarrow|100\rangle$. Subtraction of (ii) from (i) effectively gives the initial state of $I_z^0|00\rangle\langle 00|$ [Fig. 4(b) corresponding to the schematic PPS of Fig. 2(c)]. It might be noted that the method of creation of subsystem pseudopure states from cat states can also be adopted for creation of this initial state.[40]

The Hadamard gates are implemented by $(\pi/2)^{1,2}_{-y}(\pi)^{1,2}_x$ pulse (pulses are applied from left to right),[18] where $(\theta)^{1,2}_x$ denotes a θ-angle pulse (rotation) on first and second qubit about the x axis. The U_{00} operator is a controlled phase gate which can be implemented by the sequence $[(\tau/2)\times(\pi)^{1,2}_x(\tau/2)(\pi)^{1,2}_x][(\pi/2)^{1,2}_{-y}(\pi/2)^{1,2}_{-x}(\pi/2)^{1,2}_y]$, where $\tau=1/2J_{12}$.[18] The sequence $[(\tau/2)(\pi)^{1,2}_x(\tau/2)(\pi)^{1,2}_x]$ evolves the system only under the J_{12} coupling and refocuses all other couplings and proton chemical shifts,[37] whereas the $[(\pi/2)^{1,2}_{-y}(\pi/2)^{1,2}_{-x}(\pi/2)^{1,2}_y]$ is a composite z rotation on both the qubits.[41] Similarly, the other phase gates can be constructed as,[18]

$$\begin{aligned}
U_{01} &= [(\tau/2)(\pi)^{1,2}_x(\tau/2)(\pi)^{1,2}_x] \\
&\quad\times[(\pi/2)^{1,2}_{-y}(\pi/2)^{1}_x(\pi/2)^{2}_{-x}(\pi/2)^{1,2}_y], \\
U_{10} &= [(\tau/2)(\pi)^{1,2}_x(\tau/2)(\pi)^{1,2}_x] \\
&\quad\times[(\pi/2)^{1,2}_{-y}(\pi/2)^{1}_{-x}(\pi/2)^{2}_x(\pi/2)^{1,2}_y], \\
U_{11} &= [(\tau/2)(\pi)^{1,2}_x(\tau/2)(\pi)^{1,2}_x] \\
&\quad\times[(\pi/2)^{1,2}_{-y}(\pi/2)^{1,2}_x(\pi/2)^{1,2}_y].
\end{aligned} \tag{8}$$

The pulses which are simultaneously applied on both the qubits are achieved by hard pulses. However, some gates require selective excitation of qubits. Since the resonance frequencies of the two protons are relatively close to each other, selective excitation of a particular proton qubit requires long low-power pulses, which introduce significant errors in the computation.[17,19] Fortunately, in case there are two homonuclear qubits, the selective pulses can be substituted by hard pulses and delays using the variation of "jump-and-return" sequence,[42] as demonstrated by Jones and Mosca.[43] For example, the pulse sequence of U_{01} gate requires $(\pi/2)^1_x(\pi/2)^2_{-x}$ at one point. This can be achieved by using the identity[41]

$$(\pi/2)_{-y}(\pi/2)_{\pm z}(\pi/2)_y = (\pi/2)_{\pm x}. \tag{9}$$

If the proton transmitter frequency is set at the center of the spectrum, then $\nu_1=-\nu_2=\nu$, and a delay of $(1/4\nu)$ evolves the two protons under the Zeeman Hamiltonian of $2\pi\nu(I_z^1-I_z^2)$ to give the intermediate $(\pi/2)_{\pm z}$ rotation of Eq. (9). Hence,

$$(\pi/2)^1_x(\pi/2)^2_{-x} = (\pi/2)_{-y} - (1/4\nu) - (\pi/2)_y. \tag{10}$$

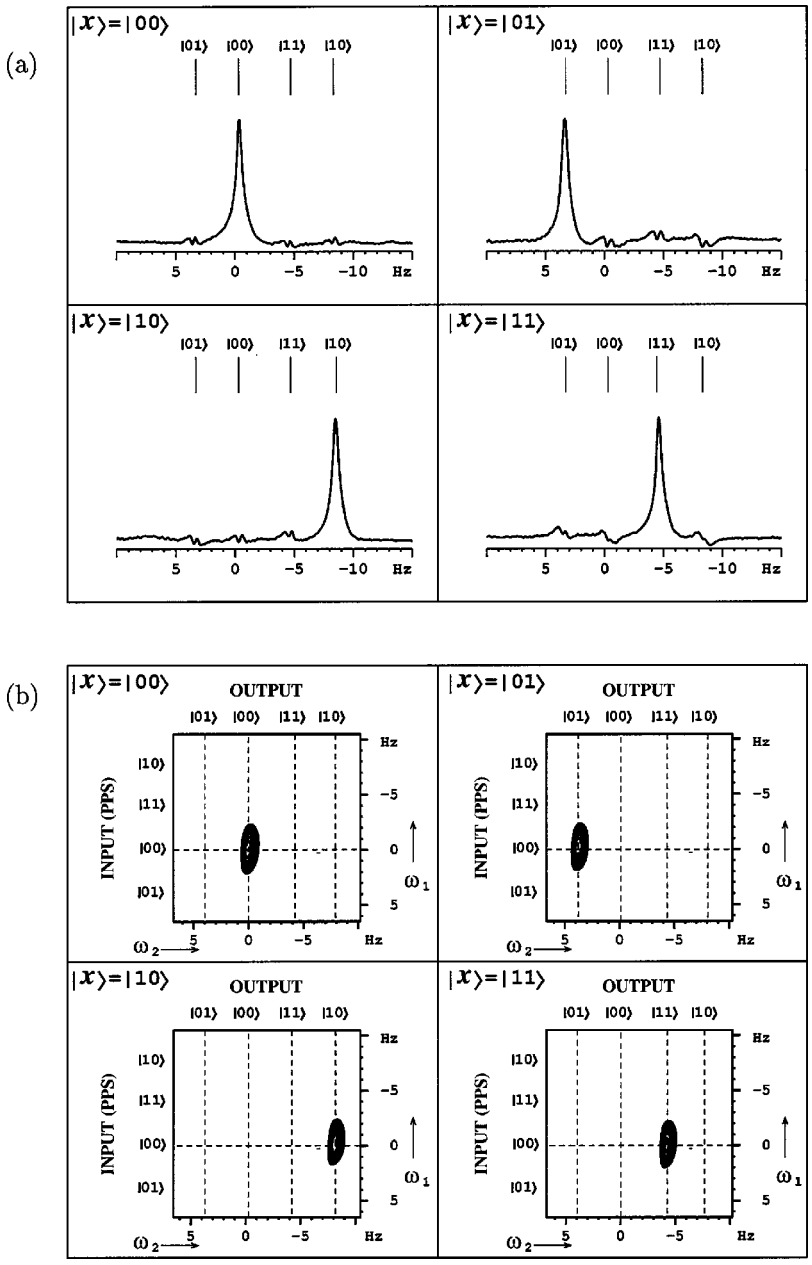

FIG. 5. (a) Spectral implementation of Grover's search algorithm by 1D experiment. After computation, the observer qubit is detected by a nonselective pulse of 14 μs. 4×1024 data points were collected and zero filled to 8×1024 before Fourier transform. The observer qubit's spectra show only the transition corresponding to the searched state ($|x\rangle$) with nonzero intensity. (b) Spectral implementation of Grover's search algorithm by 2D experiment. A 2D data set of 256×16 ($t_2 \times t_1$) was collected and zero filled to 1024×256. It may be noticed that the total size of the raw 2D dataset is of the same size as that of the 1D experiment. The doubly Fourier transformed spectra gives the input state along ω_1 and output state along ω_2.

Similarly, the pulse $(\pi/2)^1_{-x}(\pi/2)^2_x$ required for U_{10} gate, can be achieved by

$$(\pi/2)^1_{-x}(\pi/2)^2_x = (\pi/2)_y - (1/4\nu) - (\pi/2)_{-y}. \tag{11}$$

In principle, however, the evolution under J coupling during $(1/4\nu)$ would lead to some nonideal characteristics,[44] which is minimal in our system, since the ratio of maximum J coupling to chemical shift frequency difference ~1:80. This error is significantly less than the error introduced due to evolution under internal Hamiltonian during low-power long duration qubit selective pulses.

After application of the quantum circuit in Fig. 3(a) on the initial state of $I_0^z|00\rangle\langle 00|$, the observer qubit was detected by a $(\pi/2)$ pulse. From the obtained spectrum given in Fig. 5(a), one can identify the searched state ($|x\rangle$) directly. The two-dimensional experiment for spectral implementation has the added advantage that the input and output can be identified in a single spectrum. The 2D experiment of Fig. 1(b) was carried out, where during the computation period the quantum circuit of Fig. 3 was implemented on I_1 and I_2. The resultant spectrum given in Fig. 5(b), shows the input and output in each case. For example, when $|x\rangle = |11\rangle$, a cross peak at the frequency of $|00\rangle$ transition along ω_1 to that of the $|11\rangle$ transition along ω_2 identifies the input as $|00\rangle$ and the output as $|11\rangle$. The 2D spectra in Fig. 5(b) contains the initial state of $|00\rangle$ and the searched state of $|00\rangle$, $|01\rangle$, $|10\rangle$, and $|11\rangle$. In the 1D spectrum of Fig. 5(a), the initial PPS state has to be ascertained independently prior to the implementation of search algorithm.

IV. APPROXIMATE QUANTUM COUNTING

The search problem may be thought of as finding k entries out of N, which satisfy the condition $f(x)=1$. For the other, $N-k$ entries, $f(x)=0$. While Grover's search algorithm searches these k items (one at a time), quantum count-

ing finds out the value of k.[9,10] This has extreme importance because in case of multiple solutions, the required number of Grover's iteration scales as $O(\sqrt{N/k})$.[12] Hence finding out the number of existing solutions speeds up the search procedure. Moreover, the fact that counting can find out whether the number of solutions is zero or finite, makes it applicable to the nondeterministic (NP)-complete search problems, where it is important to know whether solution exists for a given search problem.[12] Approximate quantum counting has been demonstrated using NMR by Jones and Mosca.[43] In this work we provide a spectral implementation of approximate quantum counting in the three-qubit system of 4-fluro 7-nitro benzofuran, where the I^2 is the target qubit, I^1 the control qubit, and the I^0 the observed qubit.

The working of counting algorithm, as detailed by Jones and Mosca,[43] is as follows. Counting algorithm can be thought of as a method for estimating the eigenvalue of Grover's iteration $G=HU_0H^{-1}U_f$, where $U_0=I-2|00\cdots0\rangle\langle00\cdots0|$ and U_f transforms $|x\rangle$ to $(-1)^{f(x)+1}|x\rangle$. Starting from the initial $|00\cdots0\rangle$ state, an initial Hadamard on target qubit creates an uniform superposition $H|00\cdots0\rangle=(|\psi_+\rangle+|\psi_-\rangle)/\sqrt{2}$, where $|\psi_+\rangle$ and $|\psi_-\rangle$ are two eigenvectors of G.[43] These two eigenvectors are with eigenvalues of $e^{\pm i\phi_k}$, where $\sin(\phi_k/2)=\sqrt{k/N}$. An uniform superposition of the control qubit is also created. The application of controlled G produces the result

$$|\psi_+^1\rangle=(|0\rangle+e^{i\phi_k}|1\rangle)|\psi_+\rangle/\sqrt{(2)}. \tag{12}$$

If r iterations are performed, then the state is

$$|\psi_+^r\rangle=(|0\rangle+e^{ir\phi_k}|1\rangle)|\psi_+\rangle/\sqrt{(2)}. \tag{13}$$

A second Hadamard gate on the control qubit produces

$$|\psi_{f+}^r\rangle=[(1+e^{ir\phi_k})|0\rangle+(1-e^{ir\phi_k})|1\rangle]|\psi_+\rangle/2. \tag{14}$$

A similar result will happen in the case of $|\psi_-\rangle$. At the end, the final state $|\psi_f\rangle$ will be an entangled state of the control and target qubits, except when $k=0$ or $k=N$.[9,10,43]

Jones and Mosca have implemented the quantum circuit of Fig. 3(b) in a two-qubit system, measured the signal from control qubit, thereby tracing the target qubit, and shown that the signal assumes a sinusoidal behavior with r whose frequency depend on ϕ_k.[43] We have instead, started from the initial $I_z^0|00\rangle\langle00|$ state and inferred the result of counting from the spectrum of observer qubit. For a two-qubit case only one Grover's iteration is sufficient to get the result.[43] Given in Table I are the count k, their corresponding ϕ, the U_f operators, and final state of the system for $r=1$. Note that for $k=0$ the final state is $|\psi_f\rangle=|00\rangle$ and for $k=N=2$ the final state is $|\psi_f\rangle=|10\rangle$. For $k=1$ the output states are in entangled form of all the states, $|00\rangle$, $|01\rangle$, $|10\rangle$, and $|11\rangle$.

Starting with the initial state of $I_z^0|00\rangle\langle00|$, we implemented the quantum circuit of Fig. 4(b). The controlled U_0 and controlled $U_{f_{01}}$ have the same operator as that of two-qubit controlled phase gate U_{10} implemented in Grover's algorithm (Sec. II), whose corresponding pulse sequence is given in Eq. (11). $U_{f_{10}}$ has the same operator and pulse sequence as that of U_{11} in Eq. (11). $U_{f_{11}}$ is an identity operator and required no pulses. $U_{f_{00}}$ required a $(\pi)_z^1$ rotation. This $(\pi)_z^1$ rotation was implemented with hard pulses and evolution under Zeeman Hamiltonian,

$$(\pi)_z^1=(1/4\nu)-[(\pi/2)_{-y}^{1,2}(\pi/2)_x^{1,2}(\pi/2)_y^{1,2}]. \tag{15}$$

During the delay $(1/4\nu)$ the system evolves under the Zeeman Hamiltonian to acquire a rotation of $(\pi/2)_z^1(\pi/2)_{-z}^2$. The subsequent composite z pulse was applied on both qubits, $(\pi/2)_z^{1,2}=[(\pi/2)_{-y}^{1,2}(\pi/2)_x^{1,2}(\pi/2)_y^{1,2}]$, which cancels the rotation of second qubit but adds to the rotation of first qubit to give an effective $(\pi)_z^1$ rotation. It may be notied that there are two pseudo-Hadamard gates on second qubit which require spin-selective pulses since $h=(\pi/2)_y$ and $h^{-1}=(\pi/2)_{-y}$. However, these pulses can also be performed by hard pulses and evolution under Zeeman Hamiltonian using the jump-and-return logic.[43]

$$\begin{aligned}(\pi/2)_y^2&=(\pi/2)_x^{1,2}-(1/8\nu)-(\pi/2)_{-x}^{1,2}(\pi/4)_y^{1,2},\\ (\pi/2)_{-y}^2&=(\pi/2)_{-x}^{1,2}-(1/8\nu)-(\pi/2)_x^{1,2}(\pi/4)_{-y}^{1,2}.\end{aligned} \tag{16}$$

After implementing the quantum circuit of Fig. 3(b), the observer qubit was measured. The observer qubit's spectrum given in Fig. 6(a) shows four lines for $k=1$ (f_{01} and f_{10}). For $k=0$ (f_{00}) only $|00\rangle$ transition and for $k=2$ (f_{11}) only $|10\rangle$ transition is observed. The 2D-spectrum of Fig. 6(b) contains correlation of the output state with the initial $|00\rangle$ pseudopure state, and confirms the same result.

TABLE I. The various possible the count k for a two-qubit system, their corresponding ϕ, the U_f operators, and final state of the system $|\psi_{\text{output}}\rangle$.

k	ϕ_k	U_f	$\lvert\psi_{\text{output}}\rangle$
0	0	$U_{f_{00}}=\begin{pmatrix}1&0&0&0\\0&1&0&0\\0&0&-1&0\\0&0&0&-1\end{pmatrix}$	$\lvert00\rangle$
1	$\pi/2$	$U_{f_{01}}=\begin{pmatrix}1&0&0&0\\0&1&0&0\\0&0&-1&0\\0&0&0&1\end{pmatrix}$	$\lvert00\rangle-\lvert01\rangle+\lvert10\rangle+\lvert11\rangle$
1	$\pi/2$	$U_{f_{10}}=\begin{pmatrix}1&0&0&0\\0&1&0&0\\0&0&1&0\\0&0&0&-1\end{pmatrix}$	$\lvert00\rangle+\lvert01\rangle+\lvert10\rangle-\lvert11\rangle$
2	π	$U_{f_{11}}=\begin{pmatrix}1&0&0&0\\0&1&0&0\\0&0&1&0\\0&0&0&1\end{pmatrix}$	$\lvert10\rangle$

V. BERSTEIN-VAZIRANI PROBLEM

Berstein and Vazirani considered the problem of determining a n-bit string "a".[8] Classically each query would yield one bit of information and hence would require n queries to the database. However, Berstein and Vazirani showed that a quantum algorithm can solve the problem with one quantum query.[8] For this purpose, the oracle has to compute

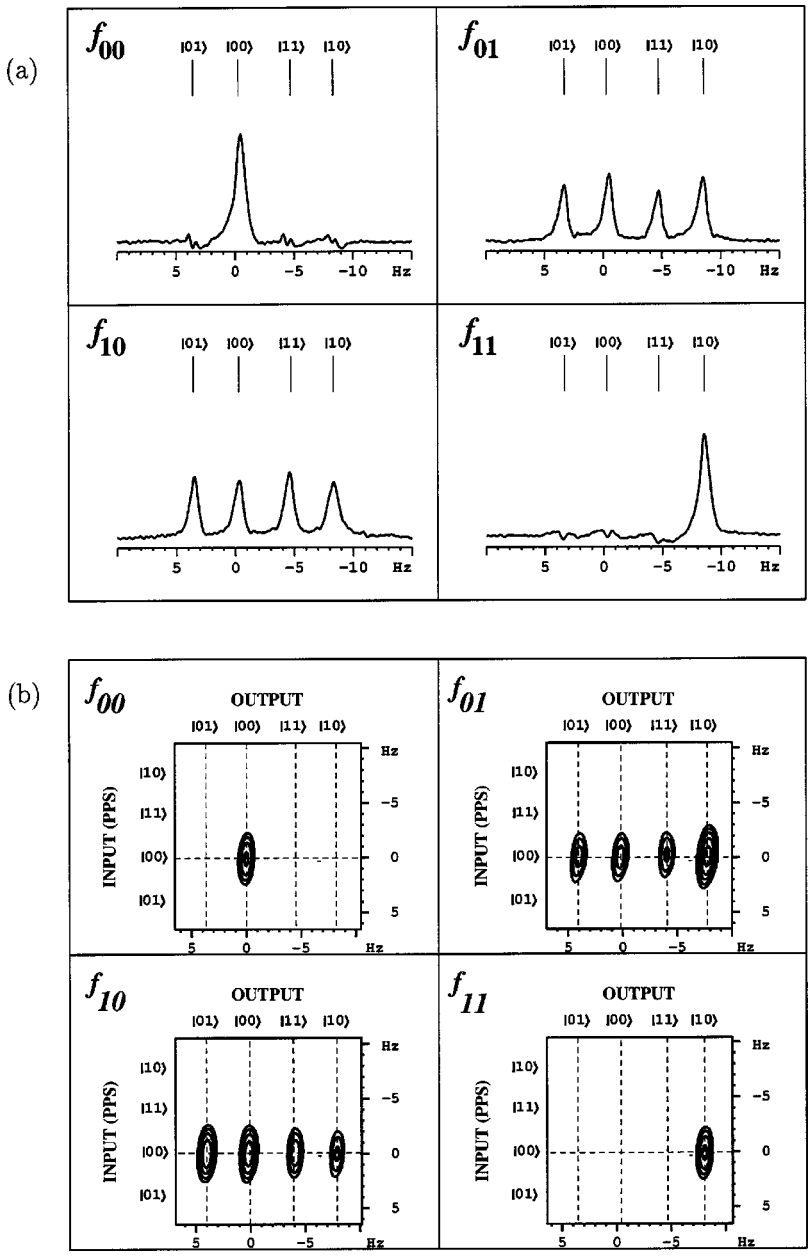

FIG. 6. (a) Spectral implementation of approximate quantum counting by 1D experiment. 4×1024 data points were collected and zero filled to 8×1024 before Fourier transform. The observer qubit's spectra show the transitions corresponding to the output state. Hence the various cases of $k=0$ (f_{00}), $k=1$ (f_{01} and f_{01}), and $k=2$ (f_{11}) can be easily identified from the spectra. (b) Spectral implementation of approximate quantum counting by 2D experiment. A 2D data set of 256×16 ($t_2\times t_1$) was collected and zero filled to 1024×256. The Fourier transformed spectra gives the output state as well as the input state.

a function $f_a(x)=ax$. The scheme proposed by Berstein and Vazirani required an ancillary qubit and determined a n-qubit string with $n+1$ qubits, which has been demonstrated by NMR recently.[36] However, Du and his co-workers had simplified the scheme such that the ancillary qubit was not required.[45] We have implemented the Du scheme, since it has the advantage of determining a n-qubit string with n-qubit system. The quantum circuit of a two-qubit implementation is given in Fig. 3(c). Starting from $|0\rangle^n$, the Hadamard gates create an uniform superposition

$$|\psi_1\rangle=\frac{1}{2^{n/2}}\sum_{x=0}^{2^n-1}|x\rangle. \tag{17}$$

The U_a operator transforms $|x\rangle\rightarrow(-1)^{f_a(s)}|x\rangle$. The unitary operator U_a can be decomposed into direct products of single-qubit operations[45]

$$U_a=U^1\otimes U^2\otimes\ldots\otimes U^n,$$

$$U^i=I,\quad a_i=0=\sigma_z,\quad a_i=1 \tag{18}$$

$$I=\begin{pmatrix}1&0\\0&1\end{pmatrix},\quad \sigma_z=\begin{pmatrix}1&0\\0&-1\end{pmatrix}.$$

Operation of U_a creates a new state $|\psi_2\rangle$ of the form,

$$|\psi_2\rangle=U_a|\psi_1\rangle=\frac{1}{2^{n/2}}\sum_{x=0}^{2^n-1}(-1)^{ax}|x\rangle. \tag{19}$$

The final state after the subsequent Hadamard operation is

$$|\psi_3\rangle=H|\psi_2\rangle=\frac{1}{2^n}\sum_{x=0}^{2^n-1}\sum_{x=0}^{2^n-1}(-1)^{ax}(-1)^{xy}|y\rangle. \tag{20}$$

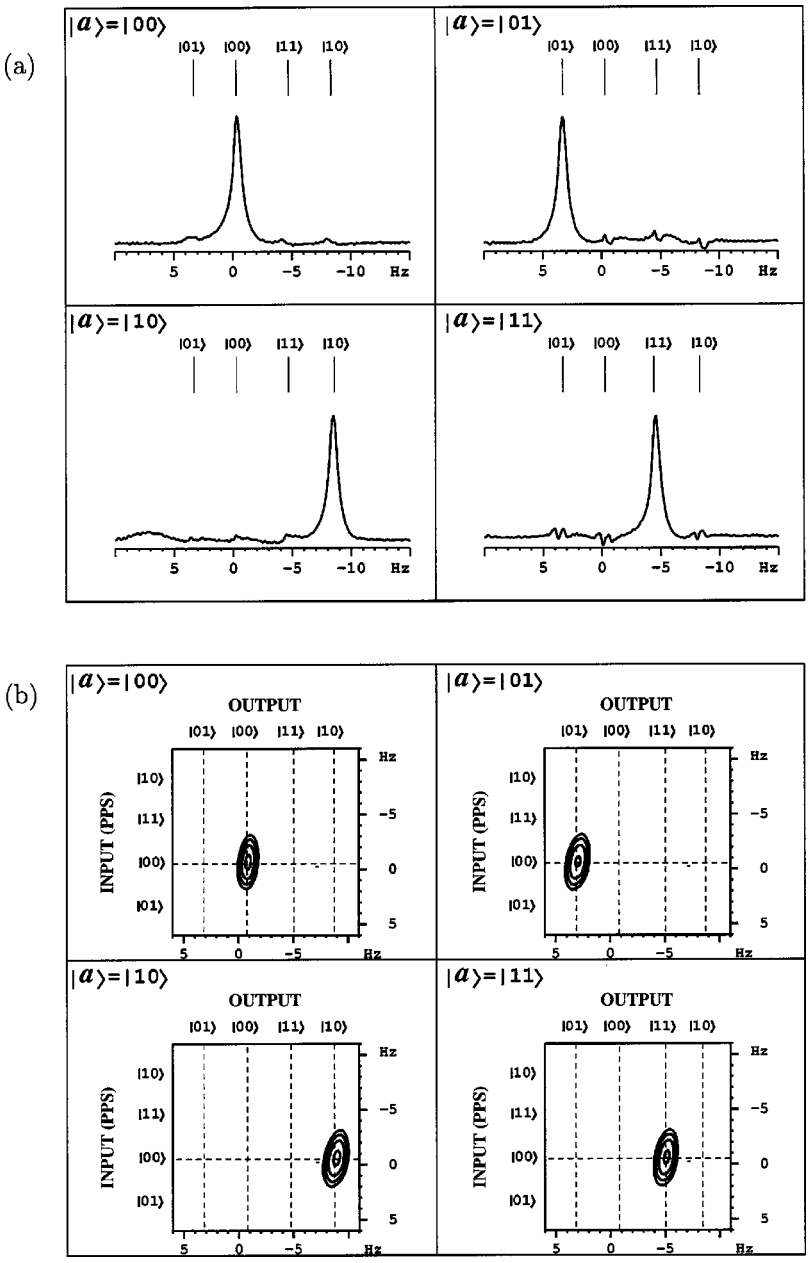

FIG. 7. (a) Spectral implementation of Berstein-Vazirani problem in a two-qubit system. The observer qubit's spectra shows the transitions corresponding to the bit string. The strings $a=00$, $a=01$, $a=10$, and $a=11$ can be identified directly from the spectra. (b) 2D spectral implementation of Berstein-Vazirani problem. A 2D data set of 256×16 ($t_2\times t_1$) was collected and zero filled to 1024×256 before Fourier transform. The Fourier transformed spectra gives the bit string against the input state in each case.

However, since $\Sigma_{x=0}^{2^n-1}(-1)^{ax}(-1)^{xy}=\delta_{a,y}$,[2] $|\psi_3\rangle=|a\rangle$.[8,43]

The algorithm was implemented to determine a two-qubit string by spectral implementation using three-qubit system of 4-fluro 7-nitro benzofuran. After creating POPS, followed by Hadamard pulses, the operator U_a was applied for $|a\rangle=|00\rangle$, $|01\rangle$, $|10\rangle$, and $|11\rangle$. U_{00} is unity operator and does not require any pulse U_{10} is σ_z^1, which requires a $(\pi)_z^1$ rotation. Once again, the $(\pi)_z^1$ rotation was implemented using the pulse sequence of Eq. (15). Similarly, U_{01} was implemented by

$$(\pi)_z^2=(\pi)_x^{1,2}(1/4\nu)(\pi)_x^{1,2}-[(\pi/2)_{-y}^{1,2}(\pi/2)_x^{1,2}(\pi/2)_y^{1,2}]. \tag{21}$$

U_{11} is $\sigma_z^1\sigma_z^2$, which can be achieved by a composite z pulse of $(\pi)_z^{1,2}=(\pi/2)_{-y}^{1,2}(\pi)_x^{1,2}(\pi/2)_y^{1,2}$. After application of the final Hadamard pulses, the observer qubit was detection by a $(\pi/2)$ pulse. The obtained spectrum given in Fig. 7(a) clearly determines the two-bit string in each case. The result of 2D experiment is given in Fig. 7(b). The 2D spectrum correlates the input $|00\rangle$ to the output in each case.

The above algorithm was also implemented to determine a three-qubit string by spectral implementation using a four-qubit system. The molecule 2-3 diflouro 6-nitrophenol (dissolved in $CDCl_3+1$ drop D_2O) has four weakly coupled spin-1/2 nuclei. The proton of the phenol group is exchanged with the D_2O. The two remaining protons and the two fluorine nuclei constitute the four-qubit system. The equilibrium spectrum of each nucleus is given in Fig. 8(a). In a 500 MHz NMR spectrometer, the chemical shift difference between the two Fluorine spins is 16 kHz while that between the two protons is 560 Hz. The couplings range from 19.13 to -2.4 Hz.

The operators and pulse sequences required for each string of a three-qubit system is given in Table II. Since the chemical shift difference between the two fluorine spins are considerably large (16 kHz), selective pulses do not intro-

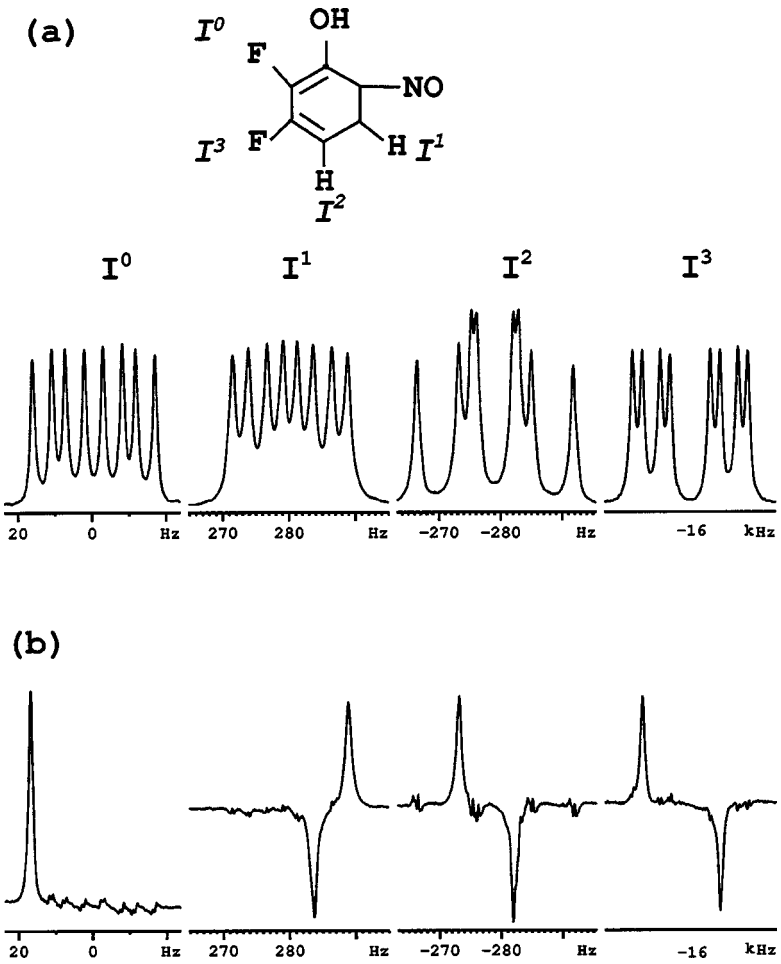

FIG. 8. (a) Chemical structure and equilibrium spectrum of 4-fluro 7-nitro benzofuran. The *J*-coupling values are $J_{01}=5.23$ Hz, $J_{02}=8.85$ Hz, $J_{03}=19.1$ Hz, $J_{12}=9.76$ Hz, $J_{13}=-2.4$ Hz, and $J_{23}=6.81$ Hz. (b) Spectra after creation of POPS. A Gaussian shaped selective pulse of 500 ms duration was applied on the $|0000\rangle\leftrightarrow|1000\rangle$ transition and the resultant spectra is subtracted from the equlibrium spectra of figure (a) to yield (b).

duce significant errors. The pulses on fluorine spin I^3 were achieved by Gaussian shaped selective pulses of 12.5 μs duration. The proton transmitter frequency was kept at the middle of the spectrum and the selective *z* pulses on protons were applied in similar logic as in the two-qubit case [Eqs. (15) and (21)]. Hard pulses were applied when both protons had to be pulsed simultaneously. The algorithm was implemented starting from the initial state of $I_z^0|000\rangle\langle 000|$ [Fig. 8(b)] and finally the observed qubit was measured by selective Gaussian shaped $(\pi/2)_y$ pulse. The only transition present in each spectrum given in Fig. 9(a) indicates the corresponding string. The 2D experimental spectra given in Fig. 9(b) verify the same results, correlating the input state of $|000\rangle$ in each case.

TABLE II. The operators and pulse sequences required for determination of each string in a three-qubit system.

String	Operator	Pulse sequence
$\|000\rangle$	I	No pulse
$\|001\rangle$	σ_z^3	$(\pi)_z^3$
$\|010\rangle$	σ_z^2	$(\pi)_z^2$
$\|011\rangle$	$\sigma_z^2\sigma_z^3$	$(\pi)_z^2(\pi)_z^3$
$\|100\rangle$	σ_z^1	$(\pi)_z^1$
$\|101\rangle$	$\sigma_z^1\sigma_z^3$	$(\pi)_z^1(\pi)_z^3$
$\|110\rangle$	$\sigma_z^1\sigma_z^2$	$(\pi)_z^{1,2}$
$\|111\rangle$	$\sigma_z^1\sigma_z^2\sigma_z^3$	$(\pi)_z^{1,2}(\pi)_z^3$

VI. HOGG'S ALGORITHM

Satisfiability (SAT) problem is one of the nondeterministic polynomial (NP) combinatorial search problems.[7] SAT problem consists of a logical formula in n variables, V_1, $V_2,\ldots,V_n$.[7] One has to find an assigment (true or false) for each variable V_i, such that it makes the formula true. The logical formula can be expressed in various equivalent forms, as conjunction of clauses, where a clause is a disjunction of some variables. A clause with *k* variables is false for exactly one set of values for its variables but true for the other 2^k-1 sets. An example of clause for $k=3$ is V_1 OR V_2 OR V_3, where the clause is *false* for only $V_1=V_2=V_3=$false. Only the assignments which satisfy all the clauses are considered as solutions.[7]

While the number of steps required by a classical algorithm increase linearly with the size of the variables,[7] Hogg's algorithm can solve 1-SAT and maximally constrained *k*-SAT problems in a single step, whatever be the size of the variable.[7] Hogg's algorithm has been succesfully implemented by NMR in a three-qubit system.[46] Here we demonstrate Hogg's algorithm by spectral implementation. The Hogg's algorithm starts by creating a uniform superposition of states by initializing from $|\psi_0\rangle=|0\rangle^{\otimes n}$ and applying Hadamard gate on all qubits $|\psi_1\rangle=H^{\otimes n}|\psi_0\rangle=2^{-n/2}\Sigma_s|s\rangle$. Let m be the number of clauses in the 1-SAT logical formula. Then the unitary operations UR are consecutively applied to yield

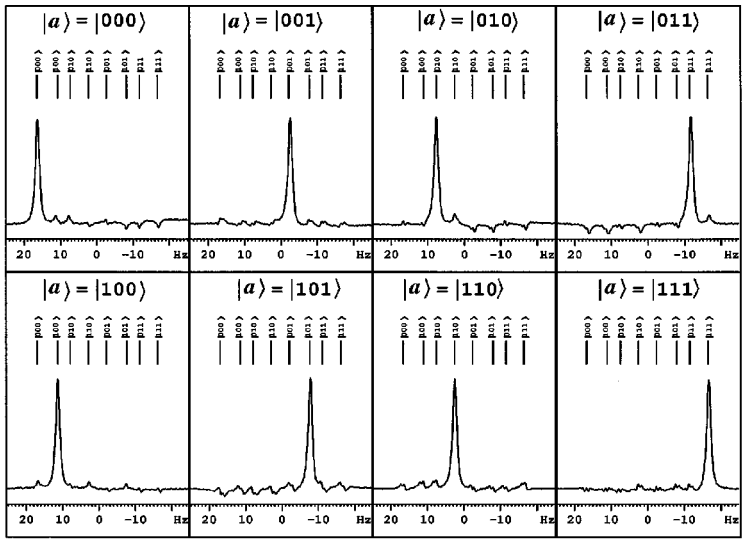

(a)

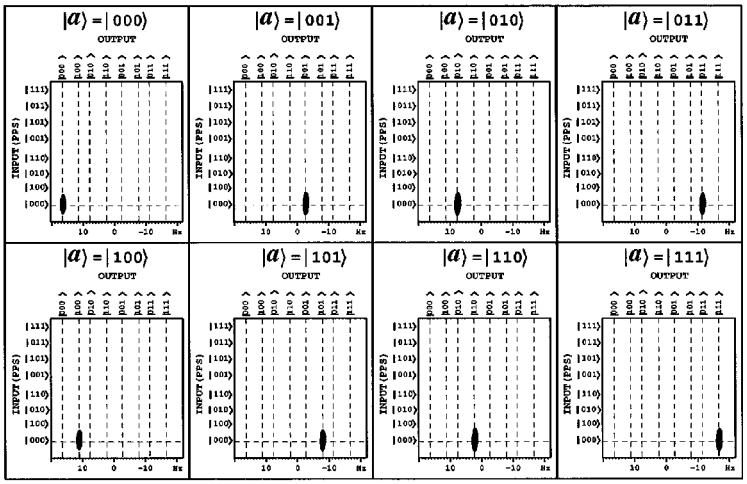

(b)

FIG. 9. (a) Spectral implementation of Berstein-Vazirani problem in a three-qubit system. After computation, the observer qubit is detected by a selective pulse of 12.5 μs duration. The observer qubit's spectra show the transitions corresponding to the bit string. The eight possible strings of $a=000$, $a=001\cdots a=111$ can be identified directly from the spectra. (b) 2D spectral implementation of Berstein-Vazirani problem in the three-qubit case. A 2D data set of 256×24 ($t_2\times t_1$) was collected and zero filled to 1024×256 before Fourier transform. The Fourier transformed spectra give the various bit strings along with the input state in each case.

TABLE III. Logic formulas for $m=1$ or $m=3$ in a three-qubit system, corresponding pulse sequences, and theoritical solutions (Ref. 45). Read the order of qubits from right to left.

m	Logic formula	Reduced pulse sequence	Final state $\lvert\psi_f\rangle$
1	$\underline{V_1}$	$(\pi)_x^1(\pi/2)_y^2(\pi/2)_y^3$	$\lvert001\rangle+\lvert011\rangle+\lvert101\rangle+\lvert111\rangle$
	V_1	$(\pi/2)_y^2(\pi/2)_y^3$	$\lvert000\rangle+\lvert010\rangle+\lvert100\rangle+\lvert110\rangle$
	$\underline{V_2}$	$(\pi/2)_y^1(\pi)_x^2(\pi/2)_y^3$	$\lvert010\rangle+\lvert011\rangle+\lvert110\rangle+\lvert111\rangle$
	V_2	$(\pi/2)_y^1(\pi/2)_y^3$	$\lvert000\rangle+\lvert001\rangle+\lvert100\rangle+\lvert101\rangle$
	$\underline{V_3}$	$(\pi/2)_y^1(\pi/2)_y^2(\pi)_x^3$	$\lvert100\rangle+\lvert101\rangle+\lvert110\rangle+\lvert111\rangle$
	V_3	$(\pi/2)_y^1(\pi/2)_y^2$	$\lvert000\rangle+\lvert001\rangle+\lvert010\rangle+\lvert011\rangle$
3	$V_3\wedge V_2\wedge \underline{V_1}$	$(\pi/2)_x^{1,2,3}(\pi/2)_{-y}^{1,2,3}(\pi/2)_x^{1,2,3}$	$\lvert111\rangle$
	$V_3\wedge \underline{V_2}\wedge V_1$	$(\pi/2)_{-x}^{1}(\pi/2)_x^{2,3}(\pi/2)_{-y}^{1,2,3}(\pi/2)_x^{1,2,3}$	$\lvert110\rangle$
	$V_3\wedge \underline{V_2}\wedge \underline{V_1}$	$(\pi/2)_x^{1,3}(\pi/2)_{-x}^{2}(\pi/2)_{-y}^{1,2,3}(\pi/2)_x^{1,2,3}$	$\lvert101\rangle$
	$\underline{V_3}\wedge V_2\wedge V_1$	$(\pi/2)_{-x}^{1,2}(\pi/2)_x^{3}(\pi/2)_{-y}^{1,2,3}(\pi/2)_x^{1,2,3}$	$\lvert100\rangle$
	$\underline{V_3}\wedge V_2\wedge \underline{V_1}$	$(\pi/2)_x^{1,2}(\pi/2)_{-x}^{3}(\pi/2)_{-y}^{1,2,3}(\pi/2)_x^{1,2,3}$	$\lvert011\rangle$
	$\underline{V_3}\wedge \underline{V_2}\wedge V_1$	$(\pi/2)_{-x}^{1,3}(\pi/2)_x^{2}(\pi/2)_{-y}^{1,2,3}(\pi/2)_x^{1,2,3}$	$\lvert010\rangle$
	$\underline{V_3}\wedge \underline{V_2}\wedge \underline{V_1}$	$(\pi/2)_x^{1}(\pi/2)_{-x}^{2,3}(\pi/2)_{-y}^{1,2,3}(\pi/2)_x^{1,2,3}$	$\lvert001\rangle$
	$V_3\wedge V_2\wedge V_1$	$(\pi/2)_{-x}^{1,2,3}(\pi/2)_{-y}^{1,2,3}(\pi/2)_x^{1,2,3}$	$\lvert000\rangle$

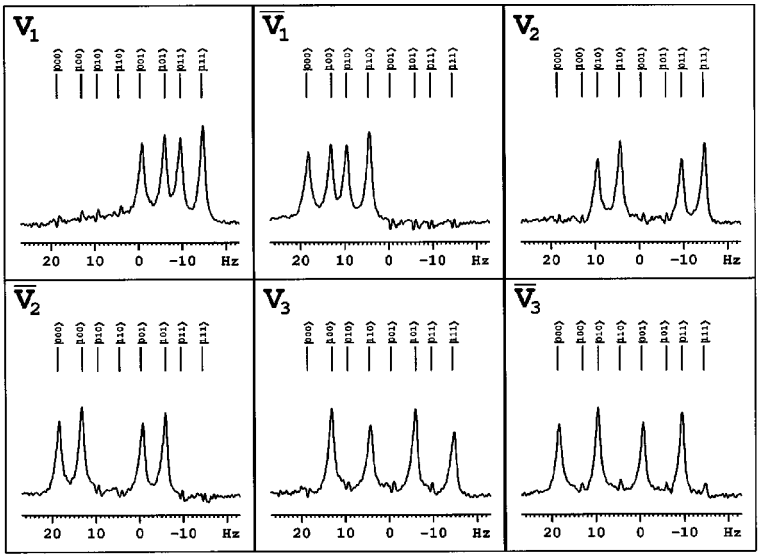

(a)

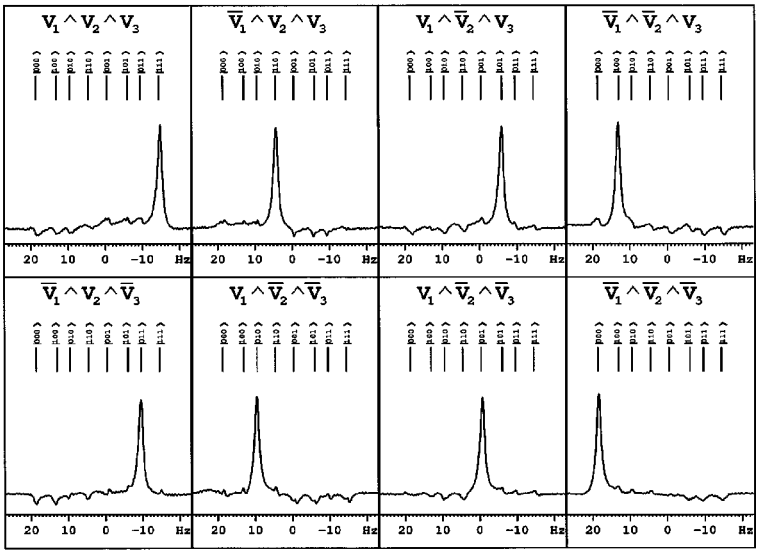

(b)

FIG. 10. One-dimensional spectral implementation of Hogg's algorithm in a three-qubit system. After computation, the observer qubit is detected by a selective pulse of 12.5 μs duration. The observer qubits spectra clearly show the output states corresponding to various logical formulas of Table III. (a) contains the spectra corresponding to $m=1$ and (b) to $m=3$.

the final state $|\psi_f\rangle = UR|\psi_1\rangle$ where U and R defined as follows. R adjusts the phases of $|s\rangle$ depending on the conflicts c of the different assignments in the superposition of s, ranging from 0 to m. R is a diagonal matrix of the form

$$\begin{aligned} R^{ss} &= \sqrt{2}\cos[(2c-1)\pi/4], \quad \text{for even } m \\ &= i^c \quad \text{for odd } m. \end{aligned} \tag{22}$$

The operator U mixes the amplitudes from different assignments with elements U_{rs}, depending on the Hamming distance d between r and s. U is of the form

$$\begin{aligned} U_{rs} &= U_{d(r,s)} \\ &= 2^{-(n-1)/2}\cos[(n-m+1-2d)\pi/4] \quad \text{for even } m \\ &= 2^{-n/2}e^{i\pi(n-m)/4}(-i)^d \quad \text{for odd } m, \end{aligned} \tag{23}$$

where $d = |r| + |s| - |r \wedge s|$ is the Hamming distance between r and s, i.e., number of positions at which their values differ. U can be decomposed into $H\Gamma H$ where H is the Hadamard matrix and Γ is a diagonal matrix of the form

$$\begin{aligned} \Gamma_{rr} &= \gamma(r) = \gamma_h \\ &= \sqrt{2}\cos[(m-2h-1)\pi/4] \quad \text{for even } m \\ &= i^h e^{-i\pi m/4} \quad \text{for odd } m, \end{aligned} \tag{24}$$

where $h = |r|$, and hence Γ_{rr} depend on the number of 1 bits in each assignment. For a detailed description of the working of the algorithm see Ref. 7. Hence the Hogg's quantum starts with the initial $|000\rangle$ state and reaches the desired output state $|\psi_f\rangle$ by

$$|\psi_f\rangle = URH|000\rangle \tag{25}$$

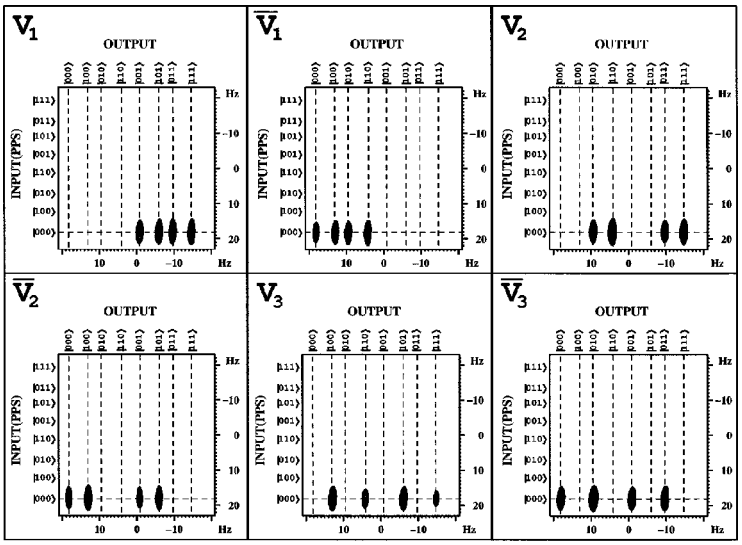

(a)

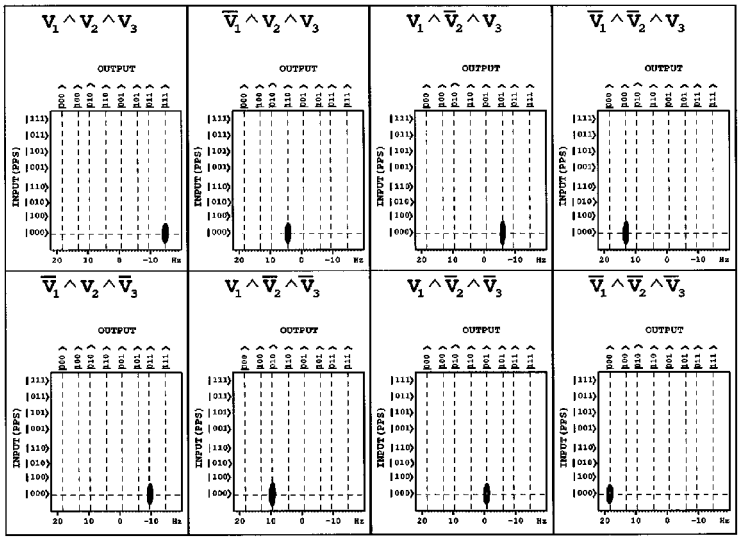

(b)

FIG. 11. Two-dimensional spectral implementation of Hogg's algorithm in a three-qubit system. The two-dimensional spectra provides the output states corresponding to various logical formulas of Table III. (a) contains the spectra corresponding to $m=1$ and (b) to $m=3$.

and the final step is to measure the output state $|\psi_f\rangle$. We have observed the final state through detection of the observer qubit.

The quantum circuit of Hogg's algorithm for a three-qubit system is given in Fig. 3(d). While implementing the corresponding pulse sequence, the consecutive pulses of opposite phases cancel out, yielding a simplified sequence.[46] The $m=1$ and 3 clauses, their logic formulas, and the reduced pulse sequences are given in Table III. Only the $m=1$ and 3 cases are demonstrated here for ease of implementation. The selective pulses on fluorine spin were achieved using Gaussian shaped pulses. In protons, the selective pulses were achieved by hard pulses concatenated with Zeeman evolution [Eqs. (10), (11), and (16)]. For example, while implementing V_1,

$$
\begin{aligned}
V_1:&[(\pi)_x^1][(\pi/2)_y^2][(\pi/2)_y^3]\\
&=[(\pi/2)_{-y}^{1,2}-1/4\nu-(\pi/2)_y^{1,2}(\pi/2)_x^{1,2}][(\pi/2)_{-x}^{1,2}-1/8\nu\\
&\quad-(\pi/2)_x^{1,2}(\pi/4)_y^{1,2}][(\pi/2)_y^3]\\
&=[(\pi/2)_{-y}^{1,2}-1/4\nu-(\pi/2)_y^{1,2}-1/8\nu\\
&\quad-(\pi/2)_x^{1,2}(\pi/4)_y^{1,2}][(\pi/2)_y^3]. \qquad (26)
\end{aligned}
$$

The spectra obtained by the one-dimensional experiment is given in Fig. 10 while the spectra obtained in 2D experiment is given in Fig. 11. The spectra of observer qubit clearly identifies the desired outputs of Table III. For example, in the case of V_1, the output has all the states that satisfy the condition that first qubit is $|1\rangle$ or false; namely, $|001\rangle$, $|011\rangle$, $|101\rangle$, and $|111\rangle$ (read the order of qubits from right to left).

Similarly, for $V_3 \wedge V_2 \wedge V_1$, the output consists of the sole answer $|111\rangle$, which satisfies the condition that all the qubits are in state $|1\rangle$.

VII. CONCLUSION

We have demonstrated spectral implementation of several quantum algorithms by one- and two-dimensional NMR. Provided future quantum computers run with high fidelity, spectral implementation delivers an aphoristic method of readout. Though it requires the use of an observer qubit, this qubit also helps in creating a pseudopure state by nonscalable and effective methods like POPS.[38] With the essentiality that the observer qubit has resolved spectrum, the principle of spectral implementation is applicable to higher qubit systems without increasing complexity.

ACKNOWLEDGMENT

Useful discussions with Professor G. S. Agarwal are gratefully acknowledged. The use of DRX-500 NMR spectrometer funded by the Department of Science and Technology (DST), New Delhi, at the Sophisticated Instruments Facility, Indian Institute of Science, Bangalore is also gratefully acknowledged. A.K. acknowledges ''DAE-BRNS'' for the award of ''Senior Scientists scheme'' and DST for a research grant for ''Quantum Computing by NMR.''

[1] R. P. Feynman, Int. J. Theor. Phys. **21**, 467 (1982).
[2] J. Preskill, *Lecture notes for Physics 229: Quantum information and Computation*, http://theory.caltech.edu/people/preskill/.
[3] S. Lloyd, Science **273**, 1073 (1996).
[4] D. Deutsch and R. Jozsa, Proc. R. Soc. London, Ser. A **400**, 97 (1985).
[5] L. K. Grover, Phys. Rev. Lett. **79**, 325 (1997).
[6] P. W. Shor, SIAM Rev. **41**, 303 (1999).
[7] T. Hogg, Phys. Rev. Lett. **80**, 2473 (1998).
[8] E. Berstein and U. Vazirani, SIAM J. Comput. **26**, 1411 (1997).
[9] M. Boyer, G. Brassard, P. Hoyer, and A. Tapp, Fortschr. Phys. **46**, 493 (1998).
[10] G. Brassard, P. Hoyer, and A. Tapp, in Automata, Languages, and Programming: Proceedings of the 25th International Colloquium, ICALP'98, Aalborg, Denmark, 1998 (Springer, Berlin, 197); quant-ph/9805082.
[11] *The Physics of Quantum Information*, edited by D. Bouwmeester, A. Ekert, and A. Zeilinger (Springer, New York, 2000).
[12] M. A. Nielsen and I. L. Chuang, *Quantum Computation and Quantum Information* (Cambridge University Press, Cambridge, 2000).
[13] D. G. Cory, A. F. Fahmy, and T. F. Havel, Proc. Natl. Acad. Sci. U.S.A. **94**, 1634 (1997).
[14] N. Gershenfeld and I. L. Chuang, Science **275**, 350 (1997).
[15] D. G. Cory, M. D. Price, and T. F. Havel, Physica D **120**, 82 (1998).
[16] I. L. Chuang, L. M. K. Vanderspyen, X. Zhou, D. W. Leung, and S. Llyod, Nature (London) **393**, 1443 (1998).
[17] J. A. Jones and M. Mosca, J. Chem. Phys. **109**, 1648 (1998).
[18] I. L. Chuang, N. Gershenfeld, and M. Kubinec, Phys. Rev. Lett. **80**, 3408 (1998).
[19] J. A. Jones, M. Mosca, and R. H. Hansen, Nature (London) **393**, 344 (1998).
[20] K. Dorai, T. S. Mahesh, Arvind, and A. Kumar, Curr. Sci. **79**, 1447 (2000).
[21] K. Dorai, Arvind, and A. Kumar, Phys. Rev. A **61**, 042306 (2000).
[22] N. Sinha, T. S. Mahesh, K. V. Ramanathan, and A. Kumar, J. Chem. Phys. **114**, 4415 (2001).
[23] Arvind, K. Dorai, and A. Kumar, Pramana **56**, 7705 (2001).
[24] L. M. K. Vanderspyen, M. Steffen, G. Breyta, C. S. Yannoni, M. H. Sherwood, and I. L. Chuang, Nature (London) **414**, 883 (2001).
[25] A. Kumar, K. V. Ramanathan, T. S. Mahesh, N. Sinha, and K. V. R. M. Murali, Pramana **59**, 243 (2002).
[26] R. Das and A. Kumar, Phys. Rev. A **68**, 032304 (2003).
[27] R. Das, A. Mitra, S. Vijaykumar, and A. Kumar, Int. J. Quantum Inf. **1**, 387 (2003).
[28] R. Das, S. Chakraborty, K. Rukmani, and A. Kumar, Phys. Rev. A **70**, 012314 (2004).
[29] J. A. Jones, in Ref. 11, chap. 5, p. 181.
[30] I. L. Chuang, N. Greshenfeld, M. Kubinec, and D. Leung, Proc. R. Soc. London, Ser. A **454**, 447 (1998).
[31] R. Das, T. S. Mahesh, and Anil Kumar, Phys. Rev. A **67**, 062304 (2003).
[32] G. M. Leskowitz and I. J. Mueller, Phys. Rev. A **69**, 052302 (2004).
[33] Z. L. Madi, R. Bruschweiler, and R. R. Ernst, J. Chem. Phys. **109**, 10603 (1998).
[34] T. S. Mahesh, K. Dorai, Arvind, and A. Kumar, J. Magn. Reson. **148**, 95 (2001).
[35] X. Peng, X. Zhu, X. Fang, M. Feng, X. Yang, M. Lin, and K. Gao, quant-ph/0202010.
[36] X. Peng, X. Zhu, X. Fang, M. Feng, M. Liu, and K. Gao, J. Chem. Phys. **120**, 3579 (2004).
[37] R. R. Ersnt, G. Bodenhausen, and A. Wokaun, *Principles of Nuclear Magnetic Resonance in One and Two Dimensions* (Oxford University Press, New York, 1987).
[38] B. M. Fung, Phys. Rev. A **63**, 022304 (2001).
[39] V. L. Ermakov and B. M. Fung, J. Chem. Phys. **118**, 10376 (2003).
[40] E. Knill, R. Laflamme, R. Martinez, and C.-H. Tseng, Nature (London) **404**, 368 (2000).
[41] R. Freeman, T. A. Frenkiel, and M. H. Levitt, J. Magn. Reson. **44**, 409 (1981).
[42] P. Platean and M. Guron, J. Am. Chem. Soc. **104**, 7310 (1982).
[43] J. A. Jones and M. Mosca, Phys. Rev. Lett. **83**, 1050 (1999).
[44] H. K. Cummins, C. Jones, A. Furze, N. F. Soffe, M. Mosca, J. M. Peach, and J. A. Jones, Phys. Rev. Lett. **88**, 187901 (2002).
[45] J. Du, M. Shi, X. Zhou, Y. Fan, B. Ye, and R. Han, Phys. Rev. A **64**, 042306 (2001).
[46] X. Peng, X. Zhu, X. Fang, M. Feng, M. Liu, and K. Gao, Phys. Rev. A **65**, 042315 (2002).